

This is a repository copy of *Plasma-Enhanced Pulsed Laser Deposition of copper oxide and zinc oxide thin films*.

White Rose Research Online URL for this paper:

<https://eprints.whiterose.ac.uk/161503/>

Version: Published Version

---

**Article:**

Rajendiran, Sudha, Meehan, David and Wagenaars, Erik [orcid.org/0000-0002-5493-3434](https://orcid.org/0000-0002-5493-3434)  
(2020) Plasma-Enhanced Pulsed Laser Deposition of copper oxide and zinc oxide thin films. RSC Advances. 065323. ISSN 2046-2069

<https://doi.org/10.1063/5.0008938>

---

**Reuse**

This article is distributed under the terms of the Creative Commons Attribution (CC BY) licence. This licence allows you to distribute, remix, tweak, and build upon the work, even commercially, as long as you credit the authors for the original work. More information and the full terms of the licence here:

<https://creativecommons.org/licenses/>

**Takedown**

If you consider content in White Rose Research Online to be in breach of UK law, please notify us by emailing [eprints@whiterose.ac.uk](mailto:eprints@whiterose.ac.uk) including the URL of the record and the reason for the withdrawal request.

# Plasma-enhanced pulsed laser deposition of copper oxide and zinc oxide thin films

Cite as: AIP Advances 10, 065323 (2020); <https://doi.org/10.1063/5.0008938>

Submitted: 26 March 2020 . Accepted: 01 June 2020 . Published Online: 19 June 2020

S. Rajendiran, D. Meehan , and E. Wagenaars 

## COLLECTIONS

Paper published as part of the special topic on [Chemical Physics](#), [Energy, Fluids and Plasmas](#), [Materials Science](#) and [Mathematical Physics](#)



View Online



Export Citation



CrossMark



## NEW: TOPIC ALERTS

Explore the latest discoveries in your field of research

**SIGN UP TODAY!**

# Plasma-enhanced pulsed laser deposition of copper oxide and zinc oxide thin films

Cite as: AIP Advances 10, 065323 (2020); doi: 10.1063/5.0008938

Submitted: 26 March 2020 • Accepted: 1 June 2020 •

Published Online: 19 June 2020



View Online



Export Citation



CrossMark

S. Rajendiran,  D. Meehan,  and E. Wagenaars<sup>a)</sup> 

## AFFILIATIONS

York Plasma Institute, Department of Physics, University of York, York YO10 5DD, United Kingdom

<sup>a)</sup> Author to whom correspondence should be addressed: [erik.wagenaars@york.ac.uk](mailto:erik.wagenaars@york.ac.uk)

## ABSTRACT

Plasma-Enhanced Pulsed Laser Deposition (PE-PLD) is a technique for depositing metal oxide thin films that combines traditional PLD of metals with a low-temperature oxygen background plasma. This proof-of-concept study shows that PE-PLD can deposit copper oxide and zinc oxide films of similar properties to ones deposited using traditional PLD, without the need for substrate heating. Varying the pressure of the background plasma changed the stoichiometry and structure of the films. Stoichiometric copper oxide and zinc oxide films were deposited at pressures of 13 Pa and 7.5 Pa, respectively. The deposition rate was  $\sim 5$  nm/min and the films were polycrystalline with a crystal size in the range of 3 nm–15 nm. The dominant phase for ZnO was (110) and for CuO, they were (020) and (11 $\bar{1}$ ), where (020) is known as a high-density phase not commonly seen in PLD films. The resistivity of the CuO film was  $0.76 \pm 0.05 \Omega \text{ cm}$ , in line with films produced using traditional PLD. Since PE-PLD does not use substrate heating or post-annealing, and the temperature of the oxygen background plasma is low, the deposition of films on heat-sensitive materials such as plastics is possible. Stoichiometric amorphous zinc oxide and copper oxide films were deposited on polyethylene (PE) and polytetrafluoroethylene (PTFE).

© 2020 Author(s). All article content, except where otherwise noted, is licensed under a Creative Commons Attribution (CC BY) license (<http://creativecommons.org/licenses/by/4.0/>). <https://doi.org/10.1063/5.0008938>

## I. INTRODUCTION

Pulsed Laser Deposition (PLD) is a well-established and widely used deposition technique for, e.g., dielectric, ferroelectric, and magnetic oxide thin films. In particular, metal-oxide wide-bandgap group II–VI semiconductors are widely studied.<sup>1,2</sup> One of the main advantages of PLD as a deposition technique is the ability to achieve stoichiometric transfer of material from the target to the substrate. However, in practice, for metal oxides, a background atmosphere of oxygen gas is often needed to avoid oxygen-deficient films that are formed under vacuum conditions.<sup>3,4</sup> In addition, the targets required are of the same complexity as the desired film, making the manufacturing of targets more demanding, compared to pure metal targets. Finally, like many other deposition techniques, PLD often requires elevated substrate temperatures, or post-annealing processes, to achieve high-quality films,<sup>3,5</sup> preventing direct deposition on heat-sensitive substrates like plastics.

In this paper, a proof-of-concept study for a modified version of PLD, Plasma-Enhanced PLD (PE-PLD),<sup>6</sup> is presented, which aims to

overcome some of the limitations of standard PLD, i.e., the need for multi-element targets and elevated substrate temperatures, for deposition metal-oxide films. The main idea is to combine a standard PLD setup using a metal target with an electrically-produced low-temperature background oxygen plasma. In this way, the sources for metal and oxygen in the deposited film are separated, similar to the approach taken in reactive magnetron sputtering techniques.<sup>7</sup> Our previous modeling investigations indicate that metal atom densities in the order of  $10^{14} \text{ cm}^{-3}$ – $10^{15} \text{ cm}^{-3}$  can be expected in the plasma plume in front of a substrate a few centimeters from the target.<sup>6</sup> In addition, a low-pressure rf-driven Inductively Coupled Plasma (ICP) used as the background plasma can provide reactive oxygen species, e.g., O and  $\text{O}_2^*$ , at densities of  $\sim 10^{14} \text{ cm}^{-3}$  to  $10^{15} \text{ cm}^{-3}$ , depending on operating conditions.<sup>6</sup> Since these densities are similar, it seems feasible that significant interaction between the plasma plume and background plasma is possible, resulting in the deposition of both metal and oxygen at comparable rates. Preliminary investigations of very thin films, 25 nm–50 nm, deposited onto quartz and analyzed with Medium Energy Ion Scattering showed broadly stoichiometric films for ZnO and  $\text{Cu}_2\text{O}$ ,<sup>8</sup> but no further

characterization of the film properties was done, nor any variation of deposition parameters. In addition, the oxygen plasma not only provides the oxygen atoms for the thin film but also provides (chemical) energy to the substrate to assist the growth of the film without additional heating of the substrate. Importantly, the oxygen plasma is a non-equilibrium, pulsed plasma to ensure that its temperature remains low,<sup>9</sup> eliminating significant conductive heating of the substrate from the plasma, potentially allowing the deposition of films onto sensitive substrates. The current paper aims to provide a more comprehensive proof-of-concept for PE-PLD of copper oxide and zinc oxide films, focusing not only on stoichiometry but also on the film structure, morphology, and film resistance. In addition, a small range of substrate materials was investigated, in particular heat-sensitive materials.

The combination of a standard PLD plume with a secondary plasma has been reported in the literature before. Notably, Dinescu *et al.* developed a plasma beam assisted PLD system in which a Zn target was ablated in standard PLD, with an additional oxygen plasma beam source also impinging on the substrate, creating ZnO films.<sup>10,11</sup> The oxygen plasma beam was generated in a separate chamber, with a beam of plasma flowing from this chamber onto the substrate, where this afterglow oxygen plasma interacted with the PLD plume and the growing film on the substrate. With this system, in combination with the substrate heating to 800 K, they achieved high-quality ZnO films. Basillais *et al.* followed a similar approach for the deposition of AlN films.<sup>12,13</sup> A pure Al target was ablated by a laser, while a nitrogen plasma was created in a separate chamber after which it flowed into the ablation chamber, interacted with the metal plasma plume, and thin film growth was achieved on heated substrates.

In our work, a similar approach is followed for separating the source of metal and oxygen to deposit metal oxide films; however, in our work no substrate heating is applied. The idea is that by using an active plasma that is in direct contact with the ablation plume, instead of an afterglow plasma beam, more reactive and energetic plasma particles impinge to the substrate. The higher energy of these particles, compared to an afterglow plasma or a neutral background gas, means that the diffusion length of these species is longer, resulting in more crystalline films.<sup>14</sup> In other words, the energy needed for good surface diffusion is provided by the background plasma rather than the heated substrate. In addition, the background plasma provides particles to the substrate for a much longer time than a laser-produced plasma plume. Tricot *et al.* showed that when using a pulsed-electron beam deposition system, plasma species are being delivered to the substrate for times much longer than those in conventional PLD, resulting in polycrystalline films deposited at room temperature, since the probability for an incoming particle to find a good site on the surface for crystalline growth is increased.<sup>15</sup> In our case, it is only the oxygen species that are delivered over a much longer time scale, but nevertheless, it can be anticipated that this can promote (poly)crystalline growth.

Huang *et al.* report ZnO films deposited at room temperature with their RF-PEPLD system<sup>16</sup> and De Giacomo *et al.* investigated TiO<sub>2</sub> films produced by Plasma-Assisted PLD.<sup>17</sup> The layout of both these systems was very similar to ours, however, for both studies, the target was a metal oxide, not a pure metal as in our case. The reason is that the main focus of their work was to reduce the droplets in the PLD plume by using a plasma background and not use the

background plasma to supply the oxygen for the film. They both showed that droplet contamination is reduced by the plasma, but at the same time, the PLD plume was still capable of depositing high-quality films. Investigations with the aim of the room-temperature deposition of metal oxide films from a metal target have not been reported to our knowledge.

The materials chosen for our proof-of-concept study are copper oxide and zinc oxide. There are two common forms of copper oxide: cuprous oxide (Cu<sub>2</sub>O) and cupric oxide (CuO). Both are *p*-type semiconductors with a bandgap of 1.9 eV–2.1 eV and 2.1 eV–2.6 eV, respectively.<sup>18</sup> Cu<sub>2</sub>O films are mainly investigated for applications in thin-film transistors (TFTs)<sup>18</sup> and solar cells.<sup>19</sup> CuO thin films find applications in gas sensors<sup>20</sup> and supercapacitors.<sup>21</sup> One of the main issues in this field is often the poor quality of the films and the high substrate temperatures that are needed for deposition. In addition, controlling the stoichiometry and obtaining single phase CuO or Cu<sub>2</sub>O has proven to be challenging.<sup>18</sup>

Zinc oxide, ZnO, is an *n*-type wide-bandgap semiconductor with a direct bandgap of ~3.3 eV that finds applications in electronic displays, thin film transistors, and solar cells.<sup>22–25</sup> Background oxygen gas pressure is known to play a crucial role in determining the surface, optical, and electrical properties of the resulting films, with the optimum pressure often being different for different types of properties.<sup>22</sup>

In this paper, a proof-of-concept study for PE-PLD of copper oxide and zinc oxide films is presented. The experimental system making the films is a combination of a standard PLD setup with a pulsed Inductively Coupled Plasma (ICP). The deposited films are characterized by Scanning Electron Microscopy (SEM), Tunneling Electron Microscopy (TEM), Selected Area Electron Diffraction (SAED), Energy Dispersive X-ray spectroscopy (EDX), X-ray Diffraction (XRD), and four-point probe resistivity measurements.

## II. EXPERIMENTAL ARRANGEMENT FOR PE-PLD

Figure 1 presents a schematic diagram of the PE-PLD setup. It consists of a standard PLD setup positioned inside a low-temperature, low-pressure ICP. The laser is a frequency-doubled, Q-switched Nd:YAG laser (Continuum Minilite II), operating at

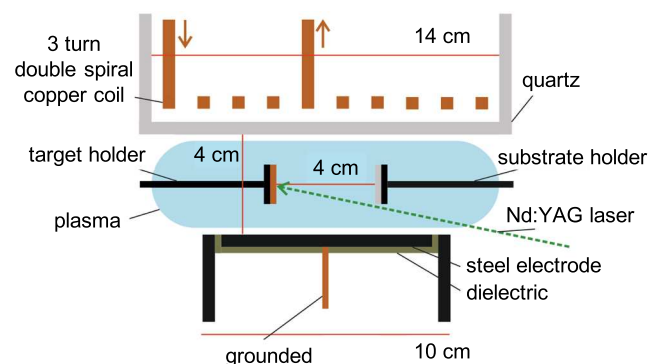


**FIG. 1.** Schematic diagram of the PE-PLD setup. A standard PLD arrangement is positioned inside a low-pressure Inductively Coupled Plasma (GEC Reference Cell). The whole setup is inside a vacuum chamber (not shown in the diagram).

532 nm, with a 5 ns pulse duration, 25 mJ pulse energy, and 10 Hz repetition rate. A wavelength of 532 nm, instead of the commonly used UV wavelengths of 355 nm or 266 nm, was chosen due to the limited laser pulse energy available to ensure sufficient fluence onto the target for a significant ablation of material. A 500 mm focal length quartz lens focuses the beam onto the rotatable Cu or Zn target (99.9% purity, Testbourne Ltd.) inside the vacuum chamber. The laser impinges the target at an angle of  $45^\circ$  to the normal and the laser fluence on the target is  $9.4 \pm 0.5 \text{ J cm}^{-2}$ . A substrate is mounted parallel to the target, at a distance of 40 mm, enough to allow sufficient plume expansion to achieve homogeneous films across the 15 mm diameter substrate area. All analyses of the deposited films were done on the central 10 mm diameter area. The substrate holder is water-cooled to 293 K. The substrate temperature was not measured directly, though the temperature of the substrate holder was monitored with a thermocouple, measuring temperatures below 300 K for all deposition conditions. Quartz is used as a substrate material for most films, apart from the films for XRD analysis of ZnO where a crystalline Si (100) wafer was used and the dedicated investigations of the deposition of films on plastics, where polyethylene (PE) and polytetrafluoroethylene (PTFE) films were used. The low-temperature ICP that is used is the inductive version of the GEC reference cell,<sup>26</sup> a standardized source widely used and characterized in the low-temperature plasma community. It consists of a three-turn double-spiral copper coil, behind a 25.4 mm thick quartz window. The bottom electrode is made of stainless steel and has a diameter of 100 mm. The distance between the quartz window and the bottom electrode is 40 mm, with the target and substrate positioned in the middle between the electrode and the quartz window, about 20 mm from the chamber central axis. The RF power is applied to the central connection of the coil, with the opposite end of the coil grounded. The driving frequency was 13.56 MHz and an L-type matching network was used for matching the effective load impedance to the RF generator impedance of 50  $\Omega$ . The ICP is operated in H-mode at pressures between 4 Pa and 25 Pa and a power of 500 W. To limit the gas temperature in the ICP, it is operated in pulsed mode, with a duty cycle of 10% and a repetition rate of 10 Hz to match the laser repetition rate. The ICP plasma pulse is synchronized with the laser using a digital delay generator (Stanford Research Systems DG 535). The laser is set to fire 8 ms after the start of each plasma pulse. The deposition time was 60 min, i.e.,  $3.6 \times 10^4$  laser shots, unless stated otherwise. This resulted in film thicknesses of around 200 nm–300 nm, depending on the ICP pressure. No substrate heating or post-annealing was carried out.

### III. RESULTS AND DISCUSSION

#### A. Stoichiometry

The stoichiometry of films deposited with the PE-PLD experimental system was investigated as a function of the oxygen ICP pressure. Since all the oxygen in the resulting films comes from the ICP, it is likely that the ICP pressure is the most sensitive control parameter for stoichiometry. Copper oxide thin films were deposited on quartz substrates, from a copper target in an oxygen ICP background, for oxygen pressures ranging from 4 Pa to 25 Pa. Zinc oxide thin films were deposited on quartz substrates, from a zinc target

with ICP oxygen pressures between 7.5 Pa and 13.5 Pa. The pressure range for copper oxide was chosen to be wider than that of zinc oxide since more stoichiometry variation is expected in copper oxide that has two common forms, CuO and Cu<sub>2</sub>O, while zinc oxide has only one, ZnO. For the EDX analysis (JEOL 7800F Prime), the electron beam energy (5 keV) was chosen such that no signal from Si in the substrate was recorded, ensuring that only the deposited films were measured. The estimated range of the penetration of the electrons was in the order of 100 nm,<sup>27</sup> while the deposited films had a thickness in the range of 200 nm–300 nm (estimated with a spectral reflectance measurement device, Filmetrics F20). EDX measurements were performed across different positions of the central 10 mm diameter area of the deposited films. No significant variations in the composition were observed for any of the films.

Figures 2 and 3 show the elemental compositions of the copper oxide and zinc oxide films, respectively, measured by EDX. For copper oxide, it is clear that the overall stoichiometry is influenced by the oxygen pressure in the ICP, with higher pressures yielding more oxygen-rich films, most likely due to a higher density of reactive oxygen species. The range of tuning is relatively large; from 80:20 Cu to O to 22:78 over a limited pressure range of 4 Pa–20 Pa. Importantly, at 13 Pa, the stoichiometry is 50:50, matching CuO. Subsequent investigations mainly focus on CuO and therefore were mostly conducted using 13 Pa oxygen pressure in the ICP.

For zinc oxide, see Fig. 3, the stoichiometry is relatively insensitive to the oxygen pressure in the ICP. For pressures 7.5 Pa and 10.5 Pa, the films are slightly oxygen deficient (53:47 and 56:44 metal to oxygen ratio, respectively), while for 13.5 Pa, the film is oxygen-rich at 47:53 metal to oxygen ratio. The limited range of stoichiometries is most likely due to the fact that there is only one form of zinc oxide (ZnO), while there are two possibilities for copper oxide, CuO and Cu<sub>2</sub>O.

The EDX results show that for both CuO and ZnO, it is possible to deposit stoichiometric films from pure metal targets using the PE-PLD technique.

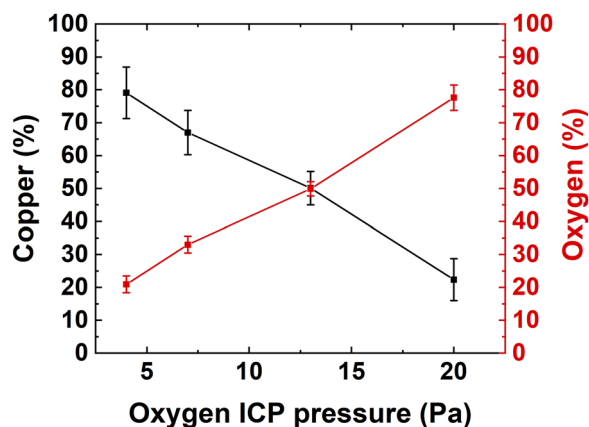
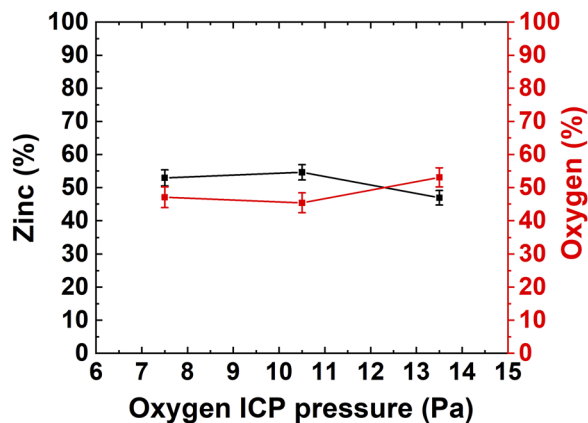


FIG. 2. Elemental composition, in atomic percentages, determined with EDX analysis, of copper-oxide films deposited by PE-PLD for different O<sub>2</sub> pressures of the ICP.



**FIG. 3.** Elemental composition, in atomic percentages, determined with the EDX analysis of zinc-oxide films deposited by PE-PLD for different O<sub>2</sub> pressures of the ICP.

### B. Structural characterization of films

In order to determine the crystal structure of the copper oxide and zinc oxide films described in Sec. III A, XRD (Rigaku Smart Lab,  $\lambda = 1.54 \text{ \AA}$ ) was performed. Figure 4 shows the measured XRD spectra for the copper oxide films as a function of ICP pressure, deposited on quartz. The signal intensity was not normalized to film thickness.

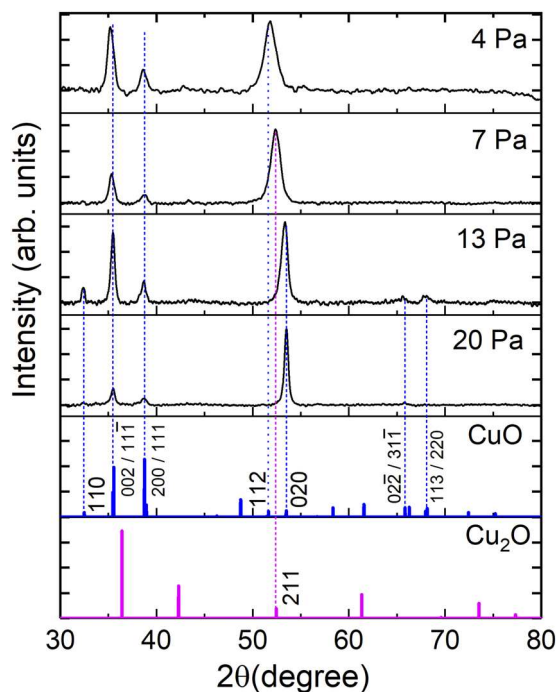


**FIG. 4.** XRD patterns of copper oxide films deposited on a quartz substrate with PE-PLD for ICP oxygen pressures in the range 4 Pa–20 Pa. Bottom two frames show reference peaks from ICDD data files 00-045-0937 for CuO and 00-005-0667 for Cu<sub>2</sub>O used for peak identification.<sup>28</sup>

The observed peaks were identified using the ICDD 00-045-0937<sup>28</sup> reference data for CuO and 00-005-0667<sup>28</sup> for Cu<sub>2</sub>O.

For all pressures, peaks at 35.5° and 38.7° are observed. These peaks correspond to CuO phases, mainly (11 $\bar{1}$ ) with a contribution from (002) and (111) with a possible smaller contribution of (200), respectively. For 13 Pa, additional CuO peaks are observed at 32.4°, corresponding to the (110) phase, at 65.7°, corresponding to a combination of (022) and (31 $\bar{1}$ ) and 68.2°, corresponding to a combination of (113) and (220) phases. Finally, the peaks in the region 51°–54° are observed for all pressures; 53.5° at 20 Pa, 53.4° at 13 Pa, 52.4° at 7 Pa, and 51.8° at 4 Pa. These peaks can be identified at the CuO (020) phase for 20 Pa and 13 Pa, the Cu<sub>2</sub>O (211) phase for 7 Pa, and the CuO (112) phase for 4 Pa.

It is clear that all of the thin films are polycrystalline, mostly CuO, which is in line with standard PLD based techniques, where it is well documented that deposited films are often polycrystalline due to the non-epitaxial nature of the deposition on quartz substrates.<sup>29</sup> For 13 Pa, observing only CuO phases is in line with the stoichiometry results from EDX (Fig. 2), giving some confidence that this film is indeed polycrystalline CuO. For 20 Pa, the measured composition suggests a Cu<sub>2</sub>O film, however, the XRD results show a combination of CuO and Cu<sub>2</sub>O structures. The presence of CuO crystals also suggests that in the remainder of this film there must be an abundance of Cu in order for the overall stoichiometry to be 2:1 Cu to O. Finally, for both 4 Pa and 20 Pa, there are some parts of the film that are polycrystalline CuO, however, based on the EDX measurements in Fig. 2, there has to be additional Cu (for 4 Pa) and O (for 20 Pa) in the remainder of the film. Therefore, the film deposited at an ICP pressure of 13 Pa seems to be the most promising in that both the stoichiometry as well as the structure are (polycrystalline) CuO. In addition, a few of the strong observed phases, e.g., the (020) phase, are known to be the high density phases, with high surface energies. These are not commonly observed with other deposition techniques, indicating that there might be significant energy transferred from the ICP to the substrate during the deposition process to allow these high-energy phases to be formed.

Figure 5 shows an XRD spectrum of the zinc oxide film deposited on the Si (100) wafer with the ICP operated at 7.5 Pa.

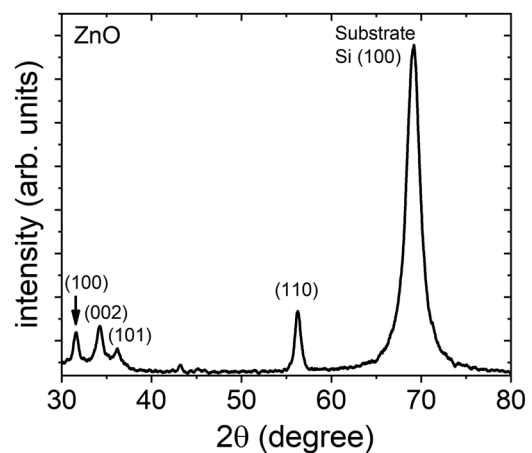


**FIG. 5.** XRD pattern of ZnO film deposited on a Si (100) substrate with PE-PLD for 7.5 Pa ICP oxygen pressure. Peaks identified with COD data file 2300112.<sup>30</sup>

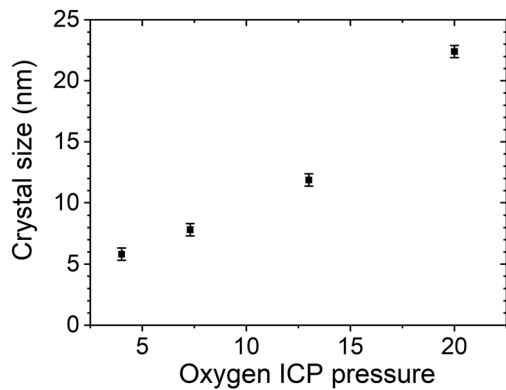


**FIG. 6.** Crystal size of copper oxide films for different ICP pressures, derived from the (002) peak in the XRD spectra using the Scherrer method.<sup>31</sup>

ZnO deposition on Si instead of quartz was chosen to avoid the overlap of the broad SiO<sub>2</sub> peak around 20° with the weak ZnO peaks in the range 30°–35°. Instead, the spectrum in Fig. 5 shows a substrate peak of Si (100) at 69.9°, away from the ZnO peaks at lower angles. The observed ZnO peaks were identified using the COD 2300112<sup>30</sup> reference data for ZnO.

The peaks in Fig. 5 at 31.6°, 32.4°, and 36.2° correspond to the (100), (002), and (101) phases of ZnO, respectively. The dominant ZnO peak in the spectrum, however, is at 56.3° corresponding to the (110) phase. The observed peaks indicate that the film is polycrystalline and has a wurtzite ZnO structure. Variation, or optimization, of the film structure with operational parameters was not performed, since this was outside the scope of this proof-of-concept study.

The crystal size of the deposited films can be estimated from the width of the measured XRD peaks using the Scherrer method.<sup>31</sup> A crystal size for the ZnO film of  $3.1 \pm 0.5$  nm was found using the (002) peak. For the copper oxide films, the crystal size was determined from the dominant (020) peak. The results are shown in Fig. 6 and it can be seen that the crystal size increases with the ICP pressure, from 5.8 nm to  $22.4 \pm 0.5$  nm. These crystal sizes are in line with

typical values for standard PLD-deposited films.<sup>32,33</sup> The increase in crystal size with a background pressure has been reported before for metal-oxide thin films<sup>34,35</sup> and can be explained by the increased interaction of the metal plume with the background plasma for increasing pressure. This leads to on average larger clusters to be formed before deposition on the surface, eventually leading to the larger crystal size in the deposited film.<sup>35</sup>

For the further investigation of the PE-PLD-deposited CuO film at 13 Pa, TEM (JEOL 2010) analysis was undertaken. For this investigation, a thinner film of about 25 nm was deposited using the same operating conditions, but at a reduced deposition time of 5 min, instead of 60 min. An ICP pressure of 13 Pa was chosen since this seemed to have the best stoichiometry and crystal structure. In preparation for the TEM analysis, protective layers of C, Pt–Pd, and Pt were deposited onto the CuO thin film. Using a Focused Ion Beam (FEI Nova Nanolab), a section of roughly 15 by 1 μm was milled out and removed from the film. This was then mounted and thinned to ~230 nm for TEM analysis. Figure 7 presents images from the TEM analysis of this sample. Figure 7(a) shows an overview of the sample, indicating the quartz substrate, CuO thin film, and the three protective layers. It also gives an indication of the homogeneity of the film thickness. Figure 7(b) presents a high magnification view showing Moiré fringes in the film due to overlapping grains and a nucleation layer of about 3 nm between the quartz substrate and the CuO film. Finally, Fig. 7(c) is a dark-field image highlighting the circular shape of the grains in the film. The grain size can be estimated as ~10 nm to 15 nm, which is in agreement with the 12 nm grain size that was derived from the XRD analysis (Fig. 6). In addition, the thickness of the film measured with the TEM was 26 nm, which means the average deposition rate was  $5.2 \pm 0.5$  nm/min, in line with what was measured for the thicker films (60 min deposition time) using a spectral reflectance measurement device.

The sample structure was investigated with Selected Area Electron Diffraction (SAED), presented in Fig. 8. A circular selected area of 138 nm diameter was investigated, shown in Fig. 8(a), consisting of the quartz substrate and part of the thin film, ~100 nm wide and 20 nm thick. The diffraction pattern in Fig. 8(b) shows a polycrystalline structure. Some of the more dominant diffraction

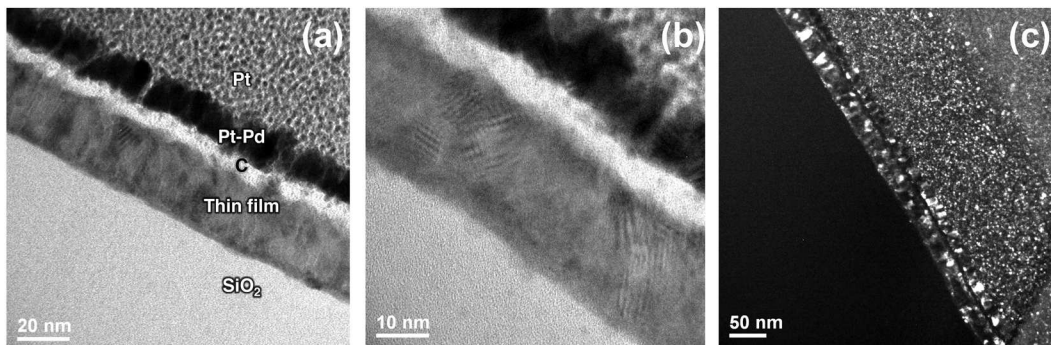


**FIG. 7.** TEM images of the CuO deposited thin film on a SiO<sub>2</sub> substrate. (a) shows the sample structure, consisting of the SiO<sub>2</sub> substrate, CuO thin film, and the C, Pt–Pd, and Pt protective layers. (b) shows a high-magnification image of the sample, focusing on the thin film and film–substrate interface. (c) is a dark-field image highlighting the grain structure in the film.

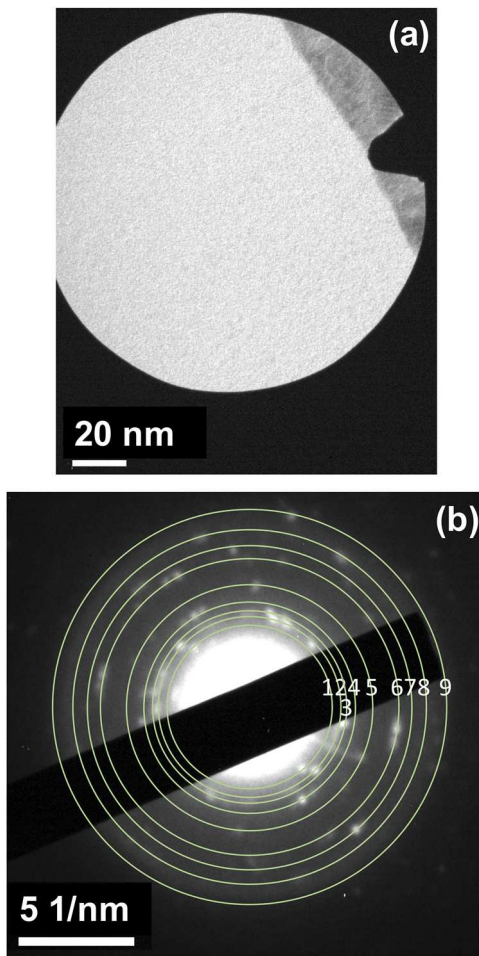


**FIG. 8.** (a) Selected Area Aperture for SAED. The bulk of the image is the quartz substrate with the thin film, ~20 nm thick, in the top right corner. (b) SAED image of the CuO deposited thin film on a SiO<sub>2</sub> substrate. Selected diffraction rings are indicated on the image, details can be found in Table I.

rings are indicated in the figure, details of which can be found in Table I. Most of the observed phases are consistent with the XRD analysis of a thicker film deposited under the same conditions (apart from deposition time). However, the SAED analysis does not show any CuO (020) phase (d spacing of 1.712 Å) that was a dominant phase in the XRD analysis. In addition, there is a Cu<sub>2</sub>O (200) phase observed in the SAED analysis, which is not present in the XRD analysis. The differences are most likely due to the fact that the films are not exactly the same (different thicknesses) and the measured area is much smaller in the case of SAED (order 100 nm diameter) compared to XRD (order 10 mm diameter). This suggests that there could be local variations in the structure of the film, which is not unlikely given the many different phases that are present in these polycrystalline films. In addition, the composition is heavily dominated by CuO phases, but there is some evidence that there are also some Cu<sub>2</sub>O grains present in the film.

**TABLE I.** SAED analysis of the CuO deposited thin film on a SiO<sub>2</sub> substrate. The ring number corresponds to the numbers in Fig. 8. Identification of diffraction rings is done with ICDD data files 00-045-0937 for CuO and 00-005-0667 for Cu<sub>2</sub>O.<sup>28</sup>

Ring number	Ring radius (nm <sup>-1</sup> )	d spacing (Å)	Identified phase
1	3.58	2.79	CuO (110)
2	3.96	2.53	CuO (11 $\bar{1}$ )/CuO (002)
3	4.21	2.37	CuO (111)/CuO (200)
4	4.61	2.17	Cu <sub>2</sub> O (200)
5	5.38	1.86	CuO (20 $\bar{2}$ )
6	6.50	1.54	CuO (11 $\bar{3}$ )/CuO (202)
7	7.08	1.41	CuO (31 $\bar{1}$ )/CuO (02 $\bar{2}$ )
8	7.74	1.29	CuO (004)/CuO (22 $\bar{2}$ )
9	8.61	1.16	CuO (222)

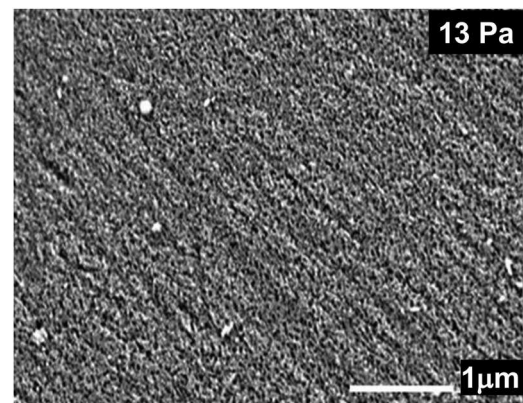
### C. Surface morphology and film resistance

Figure 9 presents an SEM image of the PE-PLD-deposited CuO film. It shows a relatively smooth surface. There is some evidence for a few particulates with a maximum size of about 100 nm–200 nm. However, no micrometer-size particulates were observed in any of the films, a known issue with standard PLD, indicating that the background plasma (or gas) is capable of preventing any particulates reaching the substrate.

Finally, the resistance of the film (60 min deposition time) was measured using a four point probe. A resistance of  $0.76 \pm 0.05 \Omega \text{ cm}$  was found, which is in line with the literature values in the range of  $0.01 \Omega \text{ cm} - 1 \Omega \text{ cm}$  for CuO thin films.<sup>36</sup>

### D. Thin film deposition on plastic substrates

Since the substrate temperature is kept low, close to ambient temperature, the deposition of thin films on heat-sensitive substrates such as plastics should be possible with PE-PLD. As a proof-of-concept, zinc oxide and copper oxide films were deposited onto PE and PTFE film substrates. The deposition conditions were 7.5 Pa O<sub>2</sub> ICP pressure, 500 W RF power, and 60 min deposition time for both the zinc and the copper cases. EDX analysis shows, within



**FIG. 9.** SEM image of the CuO deposited thin film on the SiO<sub>2</sub> substrate.

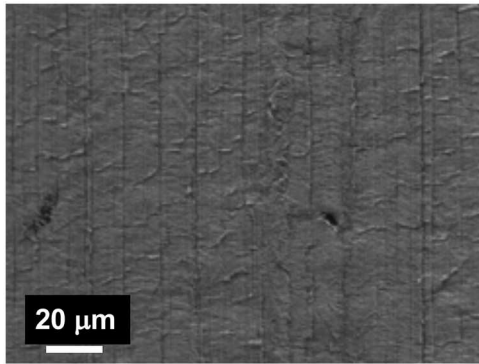


**FIG. 10.** SEM image of the copper oxide film deposited on PE at 7.5 Pa O<sub>2</sub> pressure and with 500 W RF power in the ICP. Deposition time was 60 min. The vertical ridges on the film in the SEM image originate from the PE substrate and not the copper oxide film.

error, stoichiometric ZnO films with a composition of 51:49 and 52:48 zinc to oxygen for PE and PTFE substrates, respectively. For the copper oxide samples, the stoichiometry was 67:33 and 68:32 copper to oxygen for PE and PTFE substrates, respectively. The error on all EDX measurements was  $\pm 2$  at. %. This suggests that the copper oxide film is Cu<sub>2</sub>O as was the case for the samples deposited on quartz at this pressure (Fig. 2). XRD analysis showed no metal-oxide peaks for any of the films, suggesting that they are all amorphous.

Figure 10 shows an SEM image of the copper oxide film on a PE substrate. The film appears homogeneous without any micrometer-sized particulates. The vertical ridges that can be seen originate from the structure of the PE substrate and are not a result of the film deposition process. The adhesion of the films onto the substrates was not investigated in any detail. However, it was not possible to remove the films by bending and flexing the substrates after deposition, suggesting some reasonable adhesion properties. Of course, this is only a preliminary investigation and more detailed characterization of the adhesion properties will need to be performed in the future to allow the use of these films in applications and devices.

#### IV. CONCLUSIONS

PE-PLD with a pure metal target and a background low-temperature oxygen plasma (ICP) can successfully be used to deposit copper oxide and zinc oxide thin films on a quartz substrate without external substrate heating or post-annealing. The films were polycrystalline and the stoichiometry of the copper oxide films could be tuned by varying the ICP pressure. Many of the characteristics of the deposition technique and the resulting films are similar to standard PLD using metal oxide targets and substrate heating, e.g., similar crystal size and deposition rate.<sup>29,37,38</sup> The resistivity of the film was also in line with what is reported for PLD-deposited films. The deposition of amorphous, stoichiometric zinc oxide, and copper oxide films onto the sheets of PE and PTFE was shown to be possible with PE-PLD. In conclusion, PE-PLD is capable of depositing films similar to PLD in stoichiometry and crystallinity but using pure metal targets instead of metal oxide ones and without substrate heating.

Future investigations into the performance of PE-PLD-deposited films in application-focused devices is needed to ensure that PE-PLD can indeed produce the same, or better, quality films as conventional PLD.

#### ACKNOWLEDGMENTS

The authors would like to thank Jon Barnard, Leonardo Lari, and Kevin O'Grady for their assistance with the TEM, SAED, SEM, and XRD measurements. We also acknowledge financial support from the UKRI Engineering and Physical Sciences Research Council (EPSRC), Grant No. EP/K018388/1.

#### DATA AVAILABILITY

The data that support the findings of this study are openly available in the University of York Data Catalog at <http://doi.org/10.15124/a65f4282-daae-4c90-8e3a-427085fbfee7>.

#### REFERENCES

- R. Eason, *Pulsed Laser Deposition of Thin Films: Applications-Led Growth of Functional Materials* (Wiley-Interscience, Hoboken, NJ, 2007).
- J. A. Greer, *J. Phys. D: Appl. Phys.* **47**, 034005 (2014).
- H. Christen and G. Eres, *J. Phys.: Condens. Matter* **20**, 264005 (2008).
- Z. Marton, S. S. A. Seo, T. Egami, and H. N. Lee, *J. Cryst. Growth* **312**, 2923 (2010).
- A. Singh and R. Mehra, *J. Appl. Phys.* **90**, 5661 (2001).
- S. Rajendiran, A. K. Rossall, A. Gibson, and E. Wagenaars, *Surf. Coat. Technol.* **260**, 417 (2014).
- P. Kelly and R. Arnell, *Vacuum* **56**, 159 (2000).
- A. K. Rossall, J. A. van den Berg, D. N. Meehan, S. Rajendiran, and E. Wagenaars, *Nucl. Instrum. Methods Phys. Res., Sect. B* **450**, 274–278 (2019).
- D. N. Meehan, K. Niemi, and E. Wagenaars, *Jpn. J. Appl. Phys., Part 1* **59**, SHH03 (2020).
- L. C. Nistor, C. Ghica, D. Matei, G. Dinescu, M. Dinescu, and G. Van Tendeloo, *J. Cryst. Growth* **277**, 26 (2005).
- N. Scarisoreanu, D. G. Matei, G. Dinescu, G. Epurescu, C. Ghica, L. C. Nistor, and M. Dinescu, *Appl. Surf. Sci.* **247**, 518 (2005).
- A. Basillais, C. Boulmer-Leborgne, J. Mathias, and J. Perrière, *Appl. Surf. Sci.* **186**, 416 (2002).
- A. Basillais, R. Benzerga, H. Sanchez, E. Le Menn, C. Boulmer-Leborgne, and J. Perrière, *Appl. Phys. A* **80**, 851 (2005).
- M. Nistor, N. B. Mandache, and J. Perrière, *J. Phys. D: Appl. Phys.* **41**, 165205 (2008).
- S. Tricot, C. Boulmer-Leborgne, M. Nistor, E. Millon, and J. Perrière, *J. Phys. D: Appl. Phys.* **41**, 175205 (2008).
- S.-H. Huang, Y.-C. Chou, C.-M. Chou, and V. K. S. Hsiao, *Appl. Surf. Sci.* **266**, 194 (2013).
- A. De Giacomo, V. A. Shakhatov, G. S. Senesi, and S. Orlando, *Spectrochim. Acta, Part B* **56**, 1459 (2001).
- E. Fortunato, P. Barquinha, and R. Martins, *Adv. Mater.* **24**, 2945 (2012).
- T. K. S. Wong, S. Zhuk, S. Masudy-Panah, and G. K. Dalapati, *Materials* **9**, 271 (2016).
- P. Samarasekara, N. T. R. N. Kumara, and N. U. S. Yapa, *J. Phys.: Condens. Matter* **18**, 2417 (2006).
- S. M. Pawar, J. Kim, A. I. Inamdar, H. Woo, Y. Jo, B. S. Pawar, S. Cho, H. Kim, and H. Im, *Sci. Rep.* **6**, 21310 (2016).
- Ü. Özgür, Y. I. Alivov, C. Liu, A. Teke, M. A. Reshchikov, S. Doğan, V. Avrutin, S.-J. Cho, and H. Morkoç, *J. Appl. Phys.* **98**, 041301 (2005).
- R. Kumar, G. Kumar, O. Al-Dossary, and A. Umar, *Mater. Express* **5**, 3 (2015).

- <sup>24</sup>G. Kaur, A. Mitra, and K. L. Yadav, *Prog. Nat. Sci.: Mater. Int.* **25**, 12 (2015).
- <sup>25</sup>M. Laurenti, S. Porro, C. F. Pirri, C. Ricciardi, and A. Chiolerio, *Crit. Rev. Solid State Mater. Sci.* **42**, 153 (2017).
- <sup>26</sup>P. A. Miller, G. A. Hebner, K. E. Greenberg, P. D. Pochan, and B. P. Aragon, *J. Res. Natl. Inst. Stand. Technol.* **100**, 427 (1995).
- <sup>27</sup>K. Kanaya and S. Okayama, *J. Phys. D: Appl. Phys.* **5**, 43 (1972).
- <sup>28</sup>S. Gates-Rector and T. Blanton, *Powder Diffr.* **34**, 352 (2019).
- <sup>29</sup>M. Kawwam, F. Alharbi, A. Aldwayyan, and K. Lebbou, *Appl. Surf. Sci.* **258**, 9949 (2012).
- <sup>30</sup>H. Sowa and H. Ahsbahs, *J. Appl. Crystallogr.* **39**, 169 (2006).
- <sup>31</sup>P. Scherrer, *Göttinger Nachrichten Gesell.* **2**, 98 (1918).
- <sup>32</sup>S. Kitazawa, Y. Choi, S. Yamamoto, and T. Yamaki, *Thin Solid Films* **515**, 1901 (2006).
- <sup>33</sup>S. J. Henley, M. N. R. Ashfold, and D. Cherns, *Surf. Coat. Technol.* **177-178**, 271 (2004).
- <sup>34</sup>N. R. C. Raju, K. J. Kumar, and A. Subrahmanyam, *J. Phys. D: Appl. Phys.* **42**, 135411 (2009).
- <sup>35</sup>A. Kaushal and D. Kaur, *J. Nanopart. Res.* **13**, 2485 (2011).
- <sup>36</sup>F. M. Li, R. Waddingham, W. I. Milne, A. J. Flewitt, S. Speakman, J. Dutson, S. Wakeham, and M. Thwaites, *Thin Solid Films* **520**, 1278 (2011).
- <sup>37</sup>E. Manikandan, M. K. Moodley, S. S. Ray, B. K. Panigrahi, R. Krishnan, N. Padhy, K. G. M. Nair, and A. K. Tyagi, *J. Nanosci. Nanotechnol.* **10**, 5602 (2010).
- <sup>38</sup>M. Anusha, D. Arivuoli, E. Manikandan, and M. Jayachandran, *Opt. Mater.* **47**, 88 (2015).